Journal of Molecular Liquids 446 (2026) 129292

Contents lists available at ScienceDirect

Journal of Molecular Liquids

journal homepage: www.elsevier.com/locate/molliq

Ferrocene as a non-innocent redox marker in sensors: Unveiling its role in anion binding by electronic structure calculations and experiments

Soma Keszei [a,*], Rita Skoda-Földes [b], György Lendvay [c,*]

[a] Institute of Technical Physics and Materials Science, HUN-REN Centre for Energy Research, Konkoly-Thege út 29-33, H-1121 Budapest, Hungary
[b] Research Group of Organic Synthesis and Catalysis, University of Pannonia, Egyetem u. 10, H-8200 Veszprém, Hungary
[c] Institute of Materials and Environmental Chemistry, HUN-REN Research Centre for Natural Sciences, Magyar tudósok krt. 2., H-1117 Budapest, Hungary

ARTICLE INFO

Keywords:
Ferrocene
H-bonding
Anion recognition
Density functional theory
Ureido-heterocycles

ABSTRACT

Sensing of weakly coordinating anions remains a significant challenge, due to their relatively low basicity. Our theoretical and experimental investigations show that a ferrocene moiety, incorporated into a receptor molecule not only serves as an electrochemical marker, but also able to participate in the binding of weakly coordinating anions, making possible their detection. Geometrical parameters of DFT-optimized structures of complexes, formed by the binding of $[BF_4]^-$, $[OTf]^-$ and $[CF_3CO_2]^-$ anions to the isomers of protonated 1-(4-ferrocenyl-6-phenylpyrimidin-2-yl)-3-phenylurea revealed the formation of C-H—anion hydrogen bonds between ferrocene and the O or F atoms of the coordinated anion, which is supported by bond order, QTAIM, NCI as well as chemical energy component analysis. Importantly, the computational predictions of hydrogen bond formation are corroborated by low-temperature ^{1}H NMR titration experiments, highlighting the essential role of combined experimental and theoretical investigations in accurately characterizing anion recognition processes.

1. Introduction

Although the first scientific report on artificial anion receptors was published in 1968 [1], it took another 20 years for the field of anion sensing to get the attention of the scientific community. However, in the past few decades this field has been growing relentlessly, partly because of the rapid development of the application of host-guest chemistry in analytical chemistry, partly because of the growing demand for fast and reliable methods for anion sensing [2–11].

The key properties of a chemical sensor are high selectivity towards the analyte and long-term reversibility. These can be achieved by several types of binding sites forming covalent and noncovalent bonds, the latter including ion-dipole or electrostatic interactions as well as H-bonds and H-bond induced deprotonation reactions [12,13]. Efficient receptors are based on diamides [14–16], carbazoles [17,18], squaramides [19], sulfonamides [18,20], barbiturates [21], naphtalene imides [22–24], organoboranes [25–29], diaminomethylenemalononitriles and diaminomethyleneindanediones [30], boronic acids and esters [31,32] etc., but urea and thiourea groups [33–41] are without doubt the most popular binding sites.

Beside high selectivity and affinity towards guest anions, another important issue is the conversion of the chemical information of sensing to a physical signal that needs to be measured easily, reproducibly and fast. The most favorable techniques are based on optical [42–46] or electrochemical [47,48] methods. One of the most widely used electrochemical markers is ferrocene, whose thermal stability, relatively low oxidation potential and reversible electrochemical behavior make it especially appropriate for the purpose. The binding of anions can easily be monitored by voltammetric methods through the shift it causes in the potential of the ferrocene/ferrocenium redox couple [14,33–37,49–54].

There are numerous examples of artificial anion receptors designed for the detection of strongly basic dihydrogenphosphate [36,55], carboxylate [56–58], or halide anions [35,39,54,59–61], but there are only a handful of studies [62–64] addressing the sensing of anions of strong acids (often referred to as weakly coordinating anions, WCA), such as $[BF_4]^-$, $[OTf]^-$ or $[PF_6]^-$, despite their widespread application in organic chemistry and catalysis [65]. The reason for the lack of WCA receptors is that these anions tend not to form complexes with sensor molecules, due to their relatively low basicity. Quantum chemical simulations can provide invaluable support when searching for appropriate WCA receptors.

In recent years, new approaches have emerged in designing anion sensors, to increase the binding strength of the receptors by combining several weakly bonding binding sites, for example, ordinary N—H and

* Corresponding author.
E-mail address: keszei.soma@ek.hun-ren.hu (S. Keszei).

https://doi.org/10.1016/j.molliq.2026.129292
Received 18 August 2025; Received in revised form 27 December 2025; Accepted 15 January 2026
Available online 27 January 2026

O—H hydrogen bonds with additional C_{sp2}-H, C^{+}_{sp2}-H, anion-π and π-stacking interactions [12,61,66,67]. Interestingly, several papers mention the possibility that ferrocene can play a dual role, namely, in addition to being an electrochemical "tag", it can also contribute to binding of the anion through its C_{sp2}-H bonds [53,68–71], but no studies focus on the deeper understanding of the nature of this interaction.

In our earlier experiments we have observed that ferrocene, when built into a ureidopyrimidine receptor that was found to bind strong acids primarily at the urea moiety through a coupled protonation-coordination process, played this kind of dual role, by forming C–H–anion bonds (Scheme 1) [72]. Such kind of coordination has been reported earlier by Jordan et al. [40] for a receptor not containing the ferrocene tag. The receptor they studied was able to coordinate strong acids as CF_3COOH or CCl_3COOH but it showed no sign of complex formation when CH_3SO_3H was added. In contrast, the receptor synthesized in our group forms complexes not only with CF_3COOH or CCl_3COOH but also with even stronger acids such as HOTf and HBF_4 [72]. It can be assumed that the enhanced affinity of our receptor towards poorly basic WCA guests is related to the formation of secondary interactions mentioned above. These can arise because the ferrocene and phenyl moieties of the receptor are in close proximity to the guest anions bound to the urea unit, the primary binding site (Scheme 1).

Originally, ferrocene was intended to be only a "tag" that allows one to monitor the anion recognition process via electrochemical methods. However, its dual role could be utilized in the design of anion sensors if we knew how it operates as a binding unit. This can be learnt by properly designed experiments, with indispensable help from quantum chemistry.

In this paper we report a combined experimental and computational approach to characterize the secondary interactions in complexes formed by a ferrocene-containing ureidopyrimidine receptor and anions of strong acids (CF_3SO_3H, HBF_4 and CF_3CO_2H), focusing on the role of the ferrocene unit as a binding site and highlighting the significance of weak secondary interactions.

In the following sections the results of DFT calculations are presented that indicate the formation of secondary hydrogen bonds. Then we demonstrate that the existence of such bonds is supported by NCI, QTAIM as well as chemical energy component analysis of the wave functions. Finally, low-temperature ^{1}H NMR titration results will be presented, as an experimental proof of the concept.

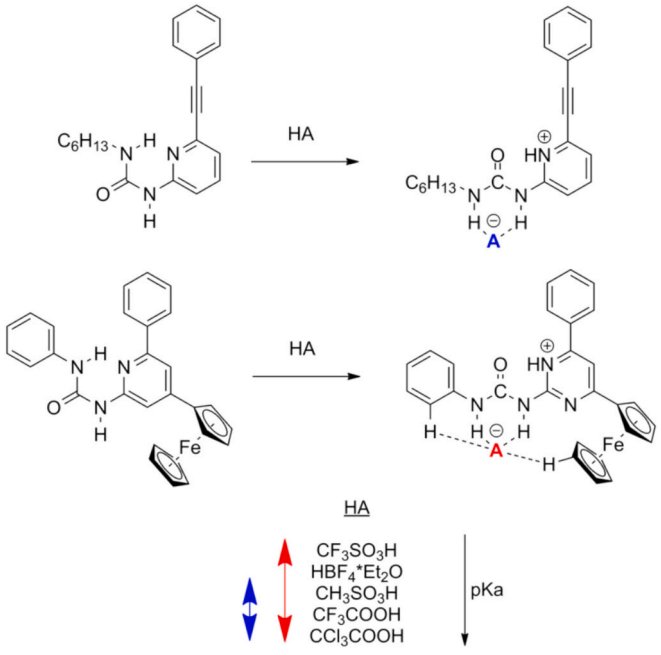

Scheme 1. Heterocyclic ureidopyrimidine derivatives as strong acid sensors coordinating anions by proton transfer and rotation of the urea unit without [40], (top and blue color) and with (bottom and red color) a ferrocene tag [72]. The bottom panel sketches the extra binding that may become possible when a ferrocene unit is present.

2. Methods

Quantum chemistry calculations. All structure determinations were performed with the Gaussian 09 software package [73]. Molecular geometries were optimized using the long-range corrected hybrid density functional CAM-B3LYP and the cc-PVDZ basis set; the properties were also evaluated at this level. We choose the CAM-B3LYP functional in our previous work [72] where we calculated UV/Vis spectra. CAM-B3LYP [74] is a long-range-corrected functional designed for the calculation of electronic spectra, and its range-correlated nature, by including exact Hartree-Fock exchange also ensures that it can quite accurately describe long-range interactions. The CAM-B3LYP/cc/pVDZ calculations provided good agreement between calculated and measured UV–Vis spectra, and together with the analysis of natural transitions orbitals [75] enabled us to assign them. The good theory-experiment agreement obtained without pseudopotentials on the iron atom suggest that the lack of the latter does not seriously influence the electronic structure of our complexes. The results concerning the geometries were also consistent with the experimental observations, including our earlier work [72,76]. To test the performance of CAM-B3LYP in geometry optimization and to make sure that no significant nonrelativistic effects are missed, all the CAM-B3LYP/cc-pVDZ optimized geometries were reoptimized at the ωB97XD/cc-pVDZ levels, and by basis sets in which the basis set of the Fe atom was replaced by the LANL2DZ basis set and pseudopotential to see possible relativistic effects. The reoptimizations introduce so small geometry changes that the energy decreased by submillihartrees only. The optimized geometries are available in the Supporting Information. The vibrational analysis of the stationary structures yielded no imaginary frequencies for the reported geometries. Verifying that each of the optimized structures are true minima on the potential energy surface. Calculations with the M05-2X functional provided very similar results.

The isotropic ^{1}H chemical shifts for the geometry-optimized structures were calculated with the gauge including atomic orbital (GIAO) method [77–79] at the CAM-B3LYP/6–311 + G(d.p) level with the SMD solvent model ($CHCl_3$), using TMS shielding calculated at the same theoretical level.

Analysis of wave functions by the Quantum Theory of Atoms in Molecules (QTAIM) and Non-Covalent Interactions (NCI) analysis were performed using the MultiWfn software (version 3.7) [80]. Multiwfn can be freely downloaded from *http://sobereva.com/multiwfn*. VMD 1.9 was used for the visualization of NCI illustrations. VMD can be freely downloaded from *https://www.ks.uiuc.edu/Research/vmd/*. Gradient isosurfaces (s = 0.6 au) are colored on a blue-green-red scale according to values of sign(λ_2)F ranging from −0.04 to 0.02 au. Blue indicates strong attractive interactions. and red indicates strong nonbonded overlap. Green color marks areas weakly attractive regions in space.

Synthesis. 1-(4-Ferrocenyl-6-phenylpyrimidin-2-yl)-3-phenylurea (**S**) was synthesized as described before [72,76].

NMR measurements. NMR experiments were carried out on a Bruker AVANCE 400 spectrometer equipped with a 5-mm BBO probe and variable temperature unit operating at ^{1}H frequency of 400.13 MHz. Chemical shifts (δ) are reported in ppm relative to the residual $CDCl_3$ signal (7.24 ppm). Dynamic NMR measurements were carried out using a dilute sample (2 mg of **S** in 500 μL $CDCl_3$) using zg pulse program with 4 s total relaxation time, spectral width of 10,000 Hz and 128 transients for each spectrum. Waiting time between temperature changes were 30 min. For the titration experiments tetrafluoroboric acid diethyl-ether complex was used for the better dissolution of the acid in chloroform and for the exclusion of water. The titrations were performed while maintaining a constant **S** concentration of 8.5 mM. The acid

concentration was varied across seven points ranging from 0 to 14.79 mM, corresponding to 0 to 1.75 equivalents (specifically 0, 0.5, 0.75, 1.0, 1.25, 1.5, and 1.75 eq.).

3. Results and discussion

The composition and the structure of our sensor molecule (1-(4-ferrocenyl-6-phenylpyrimidin-2-yl-3-phenylurea, hereafter referred to as **S**) are shown in Scheme 2. Based on our previous studies [72,76,81], two conformations can be assumed, the difference between them is that in one of the conformers (**Sa**) the ferrocene substituent, while in the other (**Sb**) the phenyl substituent of the pyrimidine ring is in the proximity of the urea moiety. Since the main binding site is the urea group, one can foresee that in conformer **Sa** there is a possibility for interaction between the coordinated anion and the ferrocene group, while in **Sb** the geometry of the molecule does not allow such an interaction. In Ref. 72 we have shown that anion binding involves a proton transfer to the sensor molecule from the acid, accompanied by the rotation of the (phenylamino)carbonyl group of the urea unit, as can be seen in Scheme 2.

3.1. Structure of the complexes – Evaluation of secondary interactions

Density-functional theory (DFT) calculations at the CAM-B3LYP/cc-pVDZ level were undertaken in order to obtain further information about the interactions governing the formation of complexes. In this section, the characteristics of the gas phase geometries are described. Note that calculations using solvent models ($CHCl_3$, CPCM and SMD) lead to similar geometries (Tables S1- S6). Implicit solvation models offer computational efficiency for large systems, the most significant limitation for WCAs is their neglect of the subtle, site-specific, non-electrostatic interactions (dispersion and weak H-bonding) between the solute and one or more solvent molecules. To ensure that no such effects are missed, we calculated the optimized geometry of **[SaH] [Y]** (Y = BF_4^-, OTf^-, $CF_3CO_2^-$ or none) with an explicit chloroform molecule (Table S7). The geometry of the complex remained essentially intact, confirming our expectation.

As it was reported before [72], the main driving force of the association of anion ($[Y]^-$) and **[SH]** $^+$ is the establishment of strong N-H—Y hydrogen bonds between the urea amide groups and the guest anion's O or F atoms (Scheme 2).

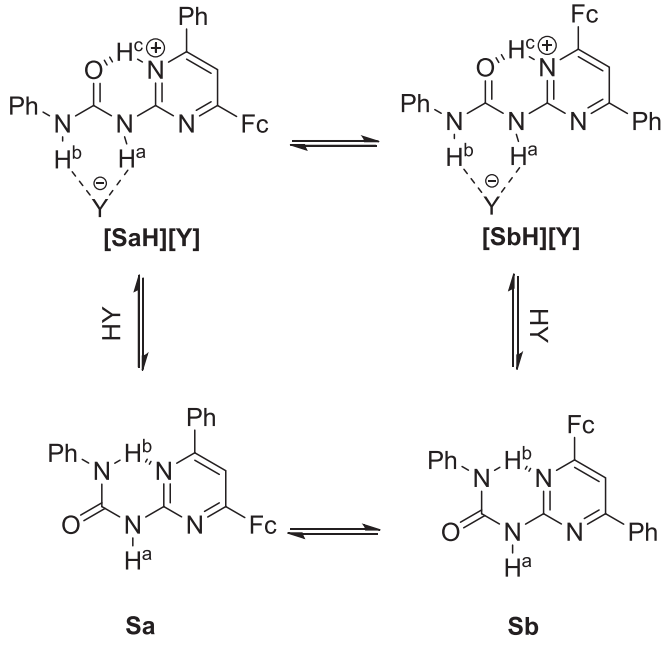

Scheme 2. Complex formation of weakly coordinating anions and conformers of the ureidopyrimdine guest (**Sa** and **Sb**) involving proton transfer and rotation of the urea unit. ($[Y]^-$ = $[OTf]^-$, $[BF_4]^-$ or $[CF_3CO_2]^-$)

However, bond distances at the optimized geometries, vibrational frequency analysis and calculated bond orders suggest that secondary interactions also affect the structure of both isomers of the complexes (Table 1). Scheme 3 presents the structures of the isomers of the complexes studied and the possible secondary H-bonding interactions in both isomers.

Inspection of the optimized geometries of the conformers **[SaH] [BF_4]**, **[SaH] [OTf]** and **[SaH] [CF_3CO_2]** in which the ferrocene unit is in the proximity of the anion shows a C_{sp2}-H—$[Y]^-$ interaction between one of ferrocene's aromatic protons and an O or F atom of the guest anions ($[Y]^-$), which is indicated by relatively short O(F)-H bond distances (denoted d(Fc—X)) of 2.155, 2.230 and 2.493 Å, in the complexes of $[BF_4]^-$, $[OTf]^-$ and $[CF_3CO_2]^-$, respectively (Fig. 1). The more basic the anion, the longer is this bond, opposite to the trend observed for the N-H—$[Y]^-$ bond lengths earlier [72], **[SaH] [CF_3CO_2]** > **[SaH] [BF_4]** > **[SaH] [OTf]**. The reason for the difference in trends is not the basicity of the anion but its geometry. In the series of these anions, a complementary effect can be observed between how favorable is the anion's geometry for the formation of the hydrogen bonds to the urea binding site and how much the geometry allows the formation of the C_{sp2}-H—$[Y]^-$ bonds to the ferrocene unit. In particular, the planar carboxylate in the $[CF_3CO_2]^-$ anion perfectly fits to the urea binding site (see Fig. 1, *iii*), forming two strong N-H—O bonds. However, there is no electronegative atom on the carbon pointing directly towards the ferrocene unit, whose cyclopentadienyl ring emerges significantly above the urea plane. Thus, ferrocene can interact only with the carboxylic O atoms, but the distance between one of the O atoms and the nearest ferrocene H atom is relatively large and the C-H—O angle is far from the ideal 180°. One can also see a C-H—F interaction between one of the F atoms of the CF_3 group and the ferrocene unit but this bond is long and the bond angle is not favorable either, which, not surprisingly, makes this bond weaker than the C-H—O bond, shown also by the smaller Mayer bond orders (Table 1). Thus, in the case of this anion, geometry favors the formation of N-H—O bonds but not the secondary hydrogen bonds to the ferrocene.

In contrast, the tetragonal structure of the units bound to the urea in the $[BF_4]^-$ and $[OTf]^-$ complexes is less favorable for the formation of the N-H—X bonds for geometrical constraints: the F—F and O—O distances do not match that of the N—N bond in urea. At the same time, a secondary hydrogen-bond can easily form, as one of the F or O atoms is

Table 1
CH—X[a] bond lengths (*d*) and angles, bond orders and C—H stretching frequencies characterizing the hydrogen bonds in the **[SaH] [Y]** complexes.

	[SaH] [BF_4]	[SaH] [OTf]	[SaH] [CF_3CO_2]	[SaH] $^+$
Fc—X[a] interaction				
d(Fc—X) /Å	2.155	2.230	2.493 (Fc—O) and 2.669 (Fc—F)	–
C-H—X angle /°	164.3	176.4	159.7 (Fc—O) and 137.3 (Fc—F)	–
ν_{as}(C—H) /cm^{-1}	3239.4	3227.0	3237.3	3249.2
ν_{as}(C—H) /cm^{-1}	3255.4	3254.5	3256.3	3266.1
ν_s(C—H) /cm^{-1}	3272.7	3272.0	3273.0	3279.8
Fc—X bond order	0.106	0.101	0.072 (Fc—O) and 0.029 (Fc—F)	–
PhA—X[a] interaction				
d(PhA—X) /Å	2.424	2.561	2.439	–
C-H—X Angle	134.1	132.3	134.2	–
PhA—X bond order	0.043	0.038	0.047	–
ν_{as}(C—H) (PhA) /cm^{-1}	3208.9	3207.5	3206.9	3186.3

[a] X = O or F.

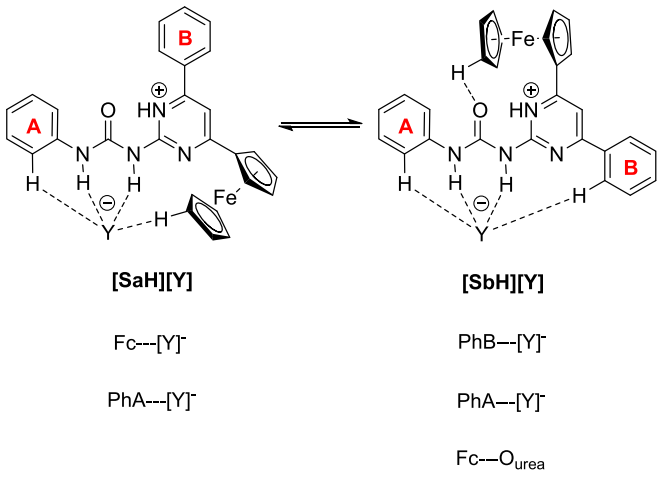

Scheme 3. Secondary interactions in the structures of **[SaH] [Y]** and **[SbH] [Y]** ($[Y]^-$ represents the anions: $[OTf]^-$, $[BF_4]^-$, $[CF_3CO_2]^-$)

out of plane and does point towards the cyclopentadienyl unit.

The formation of the C-H—O bond is reflected in the 5–17 cm^{-1} decrease of the frequencies of the C—H stretching vibration compared to the bare cation, **[SaH]** $^+$, (which appears in several normal modes because of mode–mode coupling) and in the Mayer bond orders, which are remarkably large in the complexes of $[BF_4]^-$ and $[OTf]^-$. The strength of the O(F)-H bond decreases in the order **[SaH] [BF_4]**, **[SaH] [OTf]** and **[SaH] [CF_3CO_2]**, which is reflected in the bond lengths in the series and is paralleled by the magnitude of the C—H stretching frequency reduction and the Mayer bond orders.

Another hydrogen bond can also be noticed in the complexes: it can be formed between PhA of the conformer **a** and the O or F atoms of anions, with bond distances of 2.424 Å, 2.561 Å and 2.439 Å for $[BF_4]^-$, $[OTf]^-$ and $[CF_3CO_2]^-$ respectively. However, since both the host molecule and the anion are relatively rigid and the shape of the acceptor cage allows only highly bent Y-H-C arrangements, these bonds are rather weak with Mayer bond orders around 0.04. Interestingly, the asymmetric stretching vibration of PhA increases instead of decreasing, i. e. these bonds can be classified as improper, blue-shifting hydrogen bonds [82]. The structure of complexes formed by additional anions ($[CH_3SO_3]^-$ and $[ClO_4]^-$ were also investigated. The relevant bond lengths and angles, as well as the C—H stretching frequencies related to secondary hydrogen bonds are summarized in Table S8.

Examination of the optimized structures of the complexes formed by conformer **b** of the host (shown in Table 2 and Fig. 2), **[SbH] [BF_4]**, **[SbH] [OTf]** and **[SbH] [CF_3CO_2]** in which, instead of ferrocene, the PhB phenyl ring attached to the opposite side of the pyrimidine ring is in the proximity of the guest anions. There is a chance for the formation of weak hydrogen bonds involving PhB and the electronegative atoms of the anion. This interaction is characterized by C-H—O(F) bond distances 3.171, 2.529 and 3.171 Å in complexes **[SbH] [BF_4]**, **[SbH] [OTf]** and **[SbH] [CF_3CO_2]**, respectively, reflecting that it is weak and the bonding is only remarkable in the case of the $[OTf]^-$ anion. Distances between the H atoms of PhB and the hydrogen-bond acceptor atoms of the anions doesn't follow the basicity of the guest anions here either, again due to geometrical reasons such as the large distance between the C and X and the far from linear bond angles of the possible C-H—$[Y]^-$ bonds indicate. The Mayer bond orders also show that among these interactions the only remarkable is in the complex of $[OTf]^-$ where the anion can assume the proper orientation. Similar to the complexes of conformers a, the distance between the H atom of PhA is also short enough to form a hydrogen bond with the O or F atoms of the anions, and also with the O atom of the urea group. These are also blue-shifting hydrogen bonds, and their strength is similar to those in complexes of conformer **a** (**[SbH] [BF_4]**, **[SbH] [OTf]** and **[SbH] [CF_3CO_2]**).

In the complexes of conformer **b** another interesting weak interaction can be observed, although it is not related to anion binding: the

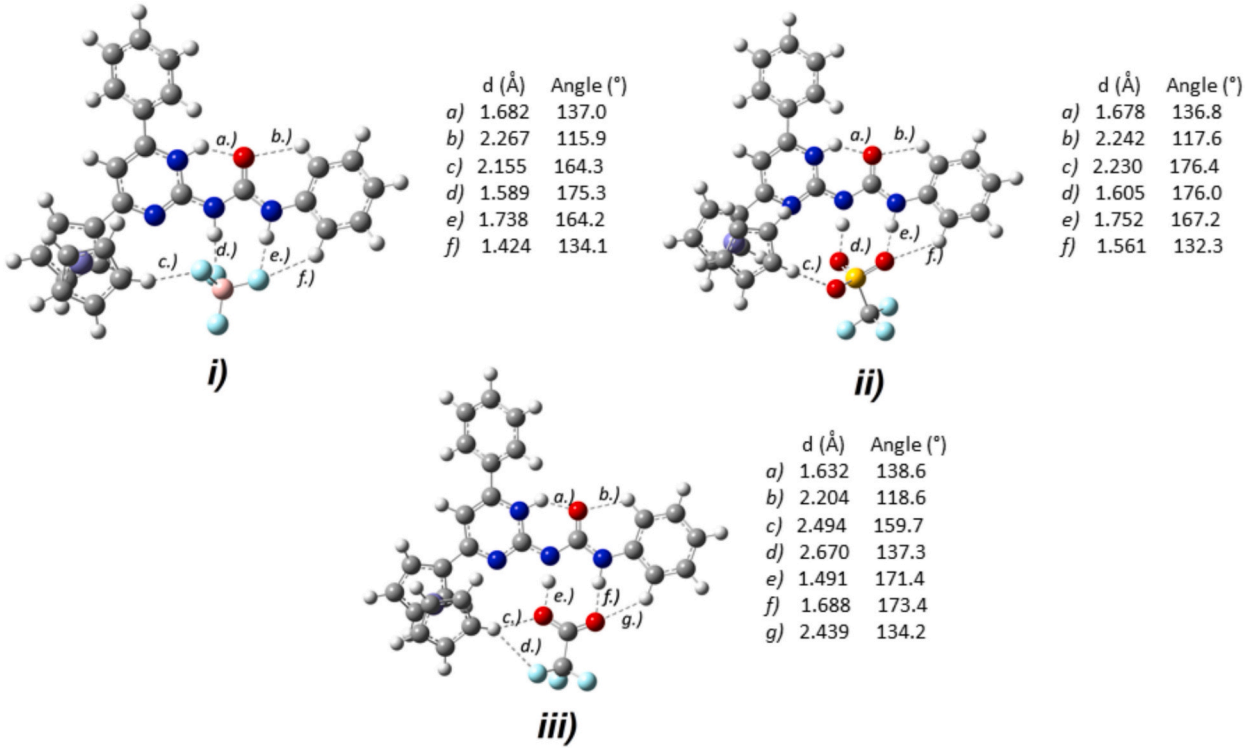

Fig. 1. Optimized geometries of *i*) **[SaH] [BF_4]**, *ii*) **[SaH] [OTf]** and *iii*) **[SaH] [CF_3CO_2]** (bottom) calculated at the CAM-B3LYP/cc-pVDZ level. Only the most important H—Y bond lengths and angles are shown. In the Supporting Information the geometry files are provided to allow the reader to view the spatial arrangements using a molecule visualization software.

Table 2
CH—X[a] bond lengths and angles, bond orders and C—H stretching frequencies characterizing the hydrogen bonds in the **[SbH] [Y]** complexes calculated at the CAM-B3LYP/cc-pVDZ level.

	[SbH] [BF_4]	**[SbH] [OTf]**	**[SbH] [CF_3CO_2]** ,	**[SbH]$^+$**
d(PhB—X) /Å	3.171	2.529	3.171	–
C-H—X angle /°	167.3	146.1	166.5	–
PhB—X bond order	0.016	0.043	0.026	–
ν_{as}(C—H) (PhB) /cm^{-1}	3205.0	3205.1	3204.2	3214.3
d(PhA—X) /Å	2.359	2.466	2.417	–
C-H—X angle /°	134.9	154.6	133.9	–
PhA—X bond order	0.048	0.046	0.048	–
ν_{as}(C—H) (PhA) /cm^{-1}	3199.2	3198.8	3197.0	3187.3

[a] X = O or F.

ferrocene moiety can get into the vicinity of the O atom of the urea group (Fig. 2), which leads to the formation of intramolecular C_{sp2}-H—O type H-bond between ferrocene and the carbonyl oxygen. The (Fc)H—O (urea) bond distances in the complexes drop by as much as 0.4 Å from that in the bare cation (Table 3), indicating that the coordination of the anions significantly enhances the strength of this hydrogen bond (which in fact is negligible in the host molecule). The frequency of the urea C═O stretching vibration decreases from the 1789.5 cm^{-1} observed in **[SbH]**$^+$ to 1760.8 cm^{-1} in the presence of the least basic anion ([BF_4]$^-$) and further to as low as 1710.3 cm^{-1} and 1710.5 cm^{-1} in the complexes of the triflate and trifluoroacetate anions, respectively. The C═O stretching frequency is related to the electron density of the urea group, which is larger in the complexes than in the bare host molecule (shown by the APT atomic charges of the urea O atom, see Table 3). The C═O bond weakens as the electron density increases, in the [BF_4]$^-$ < [OTf]$^-$ < [CF_3CO_2]$^-$ order, i.e. parallel to the basicity of the anion.

3.2. Analysis of the reduced density gradient

The geometrical properties and the changes of the vibrational frequencies as well as the Mayer bond orders strongly suggest the formation of secondary interactions between the protonated host molecules and guest anions. In order to find additional confirmation for the existence of secondary bond formation, we analyzed the wave functions. One of the methods used is based on the reduced density gradient (RDG), and identifies the regions between the assumedly noncovalently bonded atoms where the density is low and relatively flat [83,84]. These regions enclose a bond critical point (see below), which indicates the existence of a bond. Plotting the RDG isosurfaces is a useful tool to visualize those real-space regions of the complexes where weak bonding interactions (referred to noncovalent interactions, NCI by the authors of the method) are significant [83,84]. In fact, the term "noncovalent interaction" holds only in the sense that these are secondary interactions. Covalency is considered to be an interaction involving sharing of electrons, and the Mayer bond order reflects the magnitude of electron sharing. Thus, the relatively large bond order indices observed for conventional hydrogen

Table 3
CH—O bond lengths, C—H stretching frequencies, bond orders and APT charges characterizing the secondary Fc—O hydrogen bonds in the **[SbH] [Y]** complexes calculated at the CAM-B3LYP/cc-pVDZ level.

	[SbH] [BF_4]	**[SbH] [OTf]**	**[SbH] [CF_3CO_2]** ,	**[SbH]$^+$**
d(Fc—O_{urea}) /Å	2.676	2.634	2.602	3.097
ν(C=O) /cm^{-1}	1760.8	1756.1	1710.3	1789.5
ν_{as}(C—H) /cm^{-1}	3244.8	3244.6	3245.3	3245.5
ν_{as}(C—H) /cm^{-1}	3260.6	3260.2	3260.7	3263.0
ν_s(C—H) /cm^{-1}	3275.9	3275.5	3275.7	3278.6
Fc—O bond order	0.037	0.041	0.042	0.014
APT charge of O_{urea}	−0.949	−0.954	−0.971	−0.882

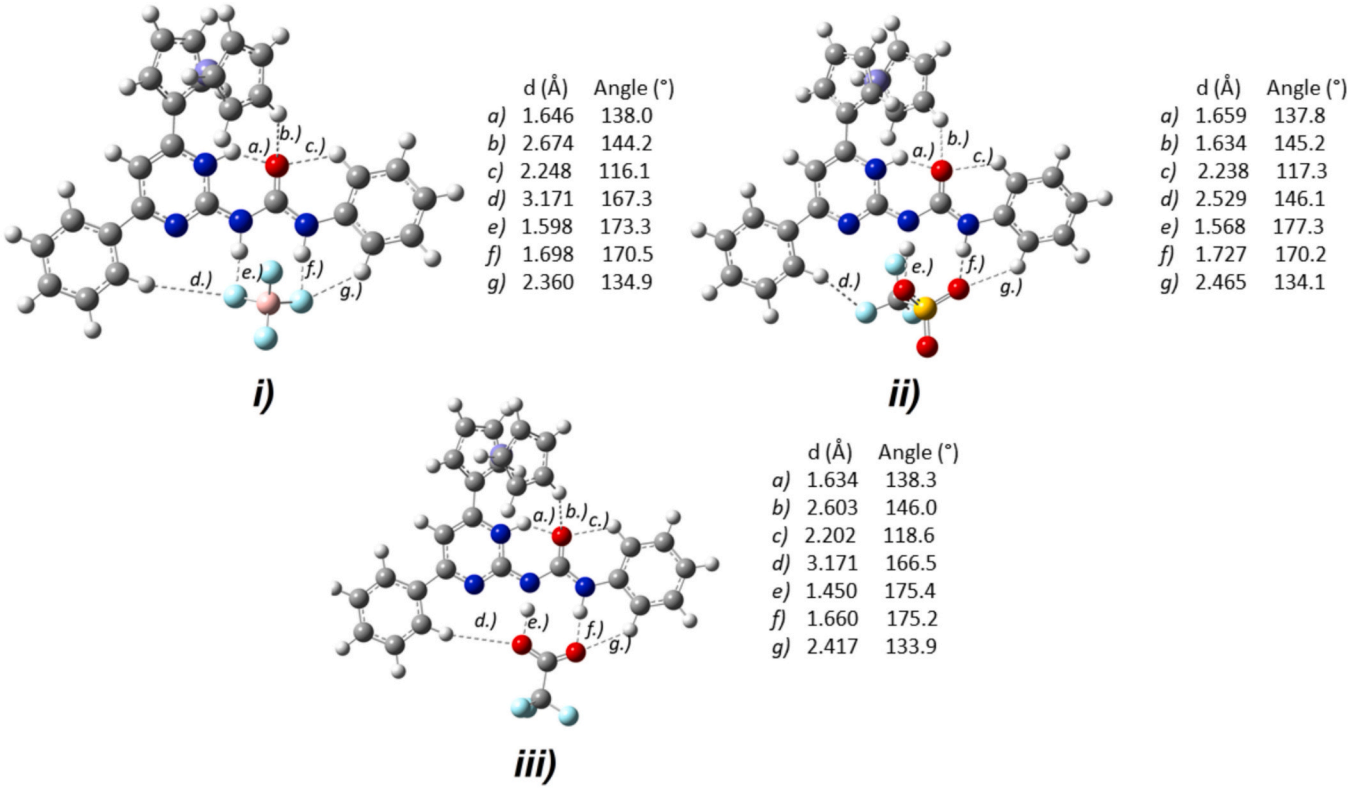

Fig. 2. Optimized geometries of *i*) **[SbH] [BF_4]** , *ii*) **[SbH] [OTf]** and *iii*)) **[SbH] [CF_3CO_2]** (bottom) calculated at the CAM-B3LYP/cc-pVDZ level.

bonds (a H-atom bridging two electronegative atoms) and smaller but non-negligible bond orders for C-H—X interactions, listed in Tables 1–3 indicate that electrons are shared between the H atom and the electronegative bridgehead atom, so that the interactions called "noncovalent" do involve covalency. Nevertheless, the NCI diagrams are good indicators for the existence of secondary bonding interactions such as hydrogen bonds. NCI diagrams of complexes **[SaH] [BF_4]**, **[SaH] [OTf]** and **[SaH] [CF_3CO_2]** (Fig. 3) clearly show the strong intermolecular hydrogen bonds between the urea NH groups and the guest anions and also the strong intramolecular bond between the pyrimidine and urea moieties marked by blue-and-red surfaces. The regions corresponding to the weak interactions identified based on geometrical parameters, vibrational frequency shifts and Mayer bond orders of the complexes (Table 1–3) can also be seen on the NCI plots. The Fc—$[Y]^-$ and PhA—$[Y]^-$ weak attractive interactions are marked by green density lobes between the O or F and the respective H atoms. In **[SaH] [CF_3CO_2]** the C_{sp2}-H—F attraction can also be noticed beside of C_{sp2}-H—O. involving the ferrocene moiety (Fig. 3). NCI visualization of the complexes of conformer **b** (Fig. 4) fully agrees with the conclusions drawn in the previous section: attractive Fc—O_{urea} and PhB—$[Y]^-$ interactions, and weaker PhA—[Y] attraction.

3.3. QTAIM analysis

The presence of weak hydrogen bonds can be supported by the analysis of the electron density based on the Quantum Theory of Atoms In Molecules (QTAIM) [85]. According to this theory, if there is a bonding interaction between two atoms, then there is a saddle point on

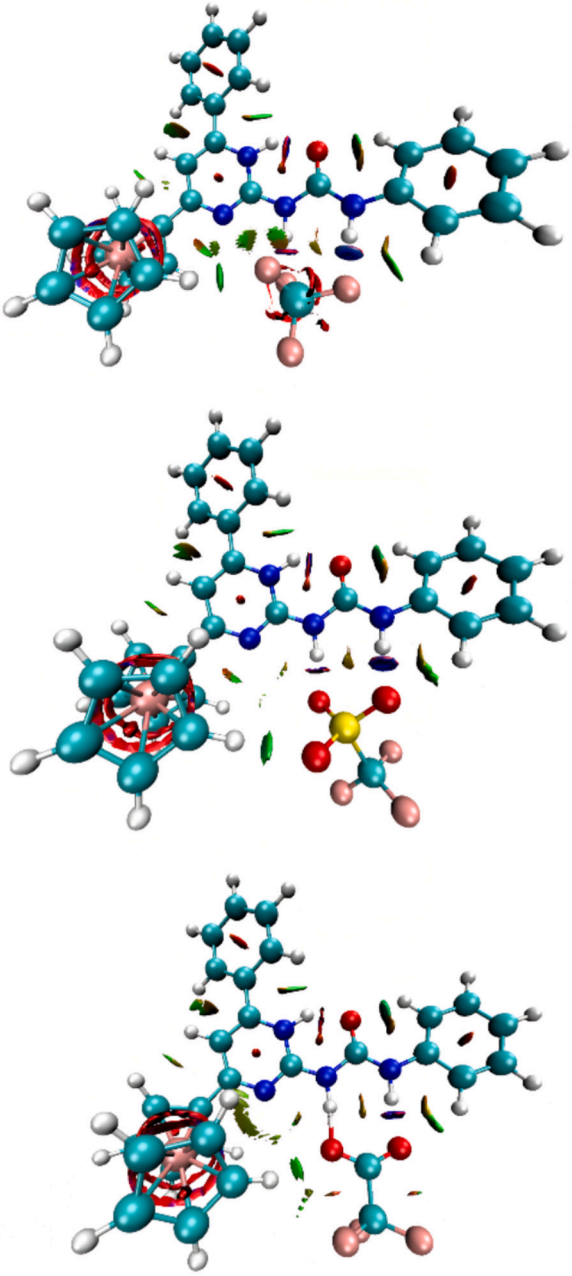

Fig. 3. NCI illustration of **[SaH] [BF_4]** (top) **[SaH] [OTf]** (middle) and **[SaH] [CF_3CO_2]** (bottom).

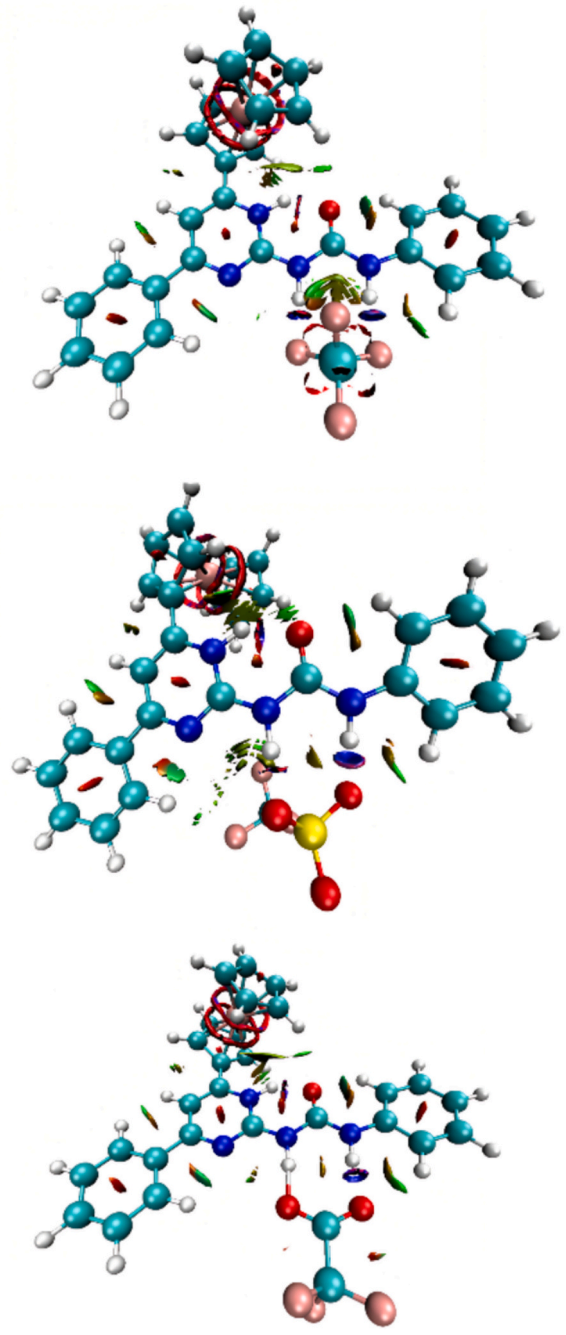

Fig. 4. NCI illustration of **[SbH] [BF_4]** (top) **[SbH] [OTf]** (middle) and **[SbH] [CF_3CO_2]** (bottom).

the electron density, the location of which is called bond critical point (BCP). Popelier [86] proposed a set of criteria for the existence of a hydrogen bond, the most important of which is the existence of a BCP between an electronegative atom and a H atom. The results of the QTAIM analysis of our complexes are shown in Fig. 5. Bond paths are established between atoms where the weak interactions - discussed earlier - occur, with a bond critical point (BCP) existing in each case. In **[SaH] [BF_4]**, **[SaH] [OTf]** and **[SaH] [CF_3CO_2]** (Fig. 5, top row) the BCPs between ferrocene's bonding H atoms and the anion's F or O atoms are well visible.

Similarly, other BCPs along the PhA—$[Y]^-$ and PhA—O_{urea} bond path of the complexes are indicative for secondary hydrogen bonds involving the phenyl moiety. In the case of **[SaH] [CF_3CO_2]** an additional BCP corresponding to an Fc—F hydrogen bond could be also observed, as expected based on the bond lengths in the optimized geometries (Table 1, Fig. 1, *iii*). In the complexes of conformer **b**, BCPs can be seen along the PhB—$[Y]^-$ bond paths for each anion, but the PhB—$[Y]^-$ interaction is so weak that with the default numerical parameters of the MultiWfn software, the corresponding bond path and BCP can be identified only in the complex of $[OTf]^-$. In contrast, the bond path and BCP between one of the Fc H atoms and the O atom of the urea unit is remarkable.

The Fc—$[Y]^-$ interactions can be characterized by electron density ($\rho(r)$), potential energy density ($V(r)$), Laplacian of electron density ($\nabla^2\rho(r)$), energy density ($H(r)$), and Lagrangian kinetic energy ($G(r)$) obtained in the BCPs (Table 4) [87,88]. The value of the $\rho(r)$ function in the bond critical point was found to be below 0.1 a.u. for the Fc—Y^- interaction for all the complexes studied, suggesting non-covalent interactions [88–90]. The small positive values of $\nabla^2\rho(r)$ at the BCPs point towards relatively weak interactions, most likely a hydrogen bond, while negative numbers would predict stronger, covalent interactions [91]. It was also reported that the values of $H(r)$ and $V(r)$ can be used to classify hydrogen bonding interactions [92]. Strong hydrogen bonds are indicated by both descriptors with negative values, while medium hydrogen bonds can be described by $\nabla 2\rho(r) > 0$ and $H(r) < 0$. On the contrary, weak hydrogen bonds can be characterized by both positive values for $H(r)$ and $\nabla^2\rho(r)$ at BCPs, predicting weak interactions for complexes **[SH] [OTf]**, **[SH] [BF_4]** and **[SH] [CF_3CO_2]**. The Electron Localization Function (ELF) [93] and the Localized Orbital Locator (LOL) [94] are functions used to provide a quantitative analysis of electron delocalization, pairing, and localization in molecules. The low values of the Electron Localization Function (ELF) and the Localized Orbital Locator (LOL) at the BCPs confirm that the region is one of electron depletion and minimal electron sharing, consistent with hydrogen-bonding interactions [89].

The empirical formula, proposed by Espinosa and coworkers [95], provides an opportunity to estimate the strength of hydrogen bonds (E_{HB}) as minus one-half of the value of the potential energy density $V(r)$) at the bond critical point (BCP)($E_{HB} = -0.5\ V(r)$). The formula predicts stronger interactions of −15.8 and − 13.4 kJ/mol for the Fc—F and Fc—O bonds in the **[SH] [BF_4]** and **[SH] [OTf]** complexes, respectively, while weaker bonds of −4.4 and − 8.0 kJ/mol for the Fc—F and Fc—O bonds in **[SH] [CF_3CO_2]**. Note that similar bond energies were reported earlier for phenyl C-H—O hydrogen bonds [90]. The obtained bonds energies are in good accordance with the geometrical parameters, characterizing the interactions, see Table 4.

3.4. Chemical energy component analysis

Among the numerous schemes designed for decomposition of the energy of a molecule [96], the Chemical Energy Component Analysis (CECA) proposed by Mayer [97–99] involves terms that can be used for identification of weak hydrogen bonds. In this method, the energy of a molecule is approximately decomposed into atomic and diatomic contributions. The diatomic contributions are further divided into terms of different physical origin [100], namely, electrostatic, exchange and overlap components and an atomic basis set extension term. The exchange component is related to electron sharing and was found to be appropriate for detecting hydrogen bonds [101,102]. We calculated the exchange contribution to the diatomic energy components of the molecule using the APOST-41 code of Mayer and Hamza [103]. We note that, unfortunately, the code is not able to handle f type atomic orbitals which prevents us from using polarization functions on the Fe atom. This is not a serious drawback because first, the decomposition is approximate anyway and second, CECA is designed to provide semiquantitative information. It would not make sense to try to find the complete basis set

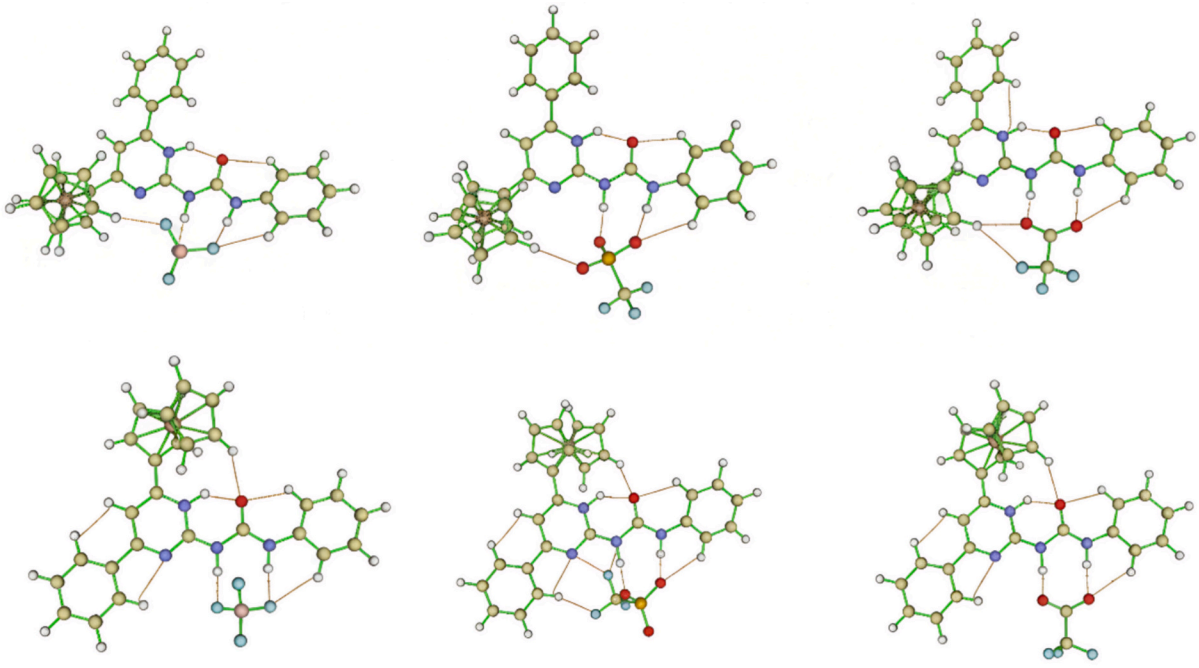

Fig. 5. The molecular representation of complexes their BCPs. BCPs are marked by a dot on the bond paths shown as orange-colored solid lines. From left to right, top: **[SaH] [BF_4]**, **[SaH] [OTf]** and **[SaH] [CF_3CO_2]** and from left to right, bottom: **[SbH] [BF_4]**, **[SbH] [OTf]** and **[SbH] [CF_3CO_2]**.

Table 4
QTAIM parameters of [SH][OTf], [SH][BF_4] and [SH][CF_3CO_2] complexes (($\rho(r)$, $\nabla 2\rho(r)$, V(r), G(r), ELF, and LOL are in a.u and E_{HB} in kJ/mol).

complex	type of bond	ρ(r)	H(r)	V(r)	$\nabla^2\rho(r)$	ELF	LOL	E_{HB}
[SH] [OTf]	C-H—O	1.4E-02	1.4E-04	-1.0E-02	4.2E-02	5.1E-02	1.9E-01	−13.4
[SH] [BF_4]	C-H—F	1.5E-02	3.1E-05	−1.2E-02	4.8E-02	4.5E-02	1.8E-01	−15.8
[SH] [CF_3CO_2]	C-H—F	4.7E-03	1.1E-03	−3.3E-03	2.2E-02	7.4E-03	8.0E-02	−4.4
[SH] [CF_3CO_2]	C-H—O	8.9E-03	2.0E-04	−6.1E-03	2.6E-02	3.0E-02	1.5E-01	−8.0

limit because of the projection operator technique used in the method. On the other hand, the tendencies such as those shown below are manifested with different basis sets the same way. We used the STO-3G and 6-31G basis sets and Hartree-Fock or CAM-B3LYP Hamiltonians. Although the numerical values differ, the tendencies were found to be identical at all levels of theory. Table 5 shows the exchange contributions for the atom pairs we monitored in the complexes of conformer **Sa**, calculated at the CAM-B3LYP/6-31G level, while those obtained at the HF/STO-3G, HF/6-31G and CAM-B3LYP/STO-3G levels are listed in Table S9.

The diatomic exchange contributions are negative. They are zero between distant atoms except occasional sub-millihartree positive or

Table 5
Exchange contributions in E_H for atom pairs in the **[SaH] [Y]** complexes, calculated at the CAM-B3LYP/6-31G level of theory.

Anion	$[OTf]^-$	$[BF_4]^-$	$[CF_3CO_2]^-$
	X---H (H-bond)		
1	-0.0313	-0.0383	-0.0556
2	-0.0195	-0.0266	-0.0357
3	-0.0292	-0.0294	-0.0332
4	-0.0043	-0.0038	-0.0049
5	-0.0024	-0.0038	-0.0035
6	-0.0055	-0.0103	-0.0048
6'	-	-	-0.0018
	C–H_R (---X). R=Fc. Ph		
7	-0.2598	-0.2587	-0.2623
8	-0.2680	-0.2674	-0.2669
	Z-X bonds in Z-X---H-N bridges		
	S-O	B-F	C-O
9	-0.2750	-0.1950	-0.4220
10	-0.2845	-0.2092	-0.4630
	Z-X bonds in Z-X---H-C bridges		
	S-O_c	B-F_c	C-F_c
11	-0.3269	-0.2342	-0.2781
	"Free" C–H bonds [a]		
PhC-H	-0.2727	-0.2727	-0.2728
PhC-H	-0.2731	-0.2730	-0.2744
PhC-H	-0.2744	-0.2744	-0.2731
Fc C-H	-0.2735	-0.2731	-0.2734
Fc C-H	-0.2732	-0.2733	-0.2733
	X–H(remote) bonds		
X_aH	-0.0005	-0.0002	-0.0001
	"Free" Z–F bonds (Z = B/C) [b]		
Z–F	-	-0.2796	-0.2849
Z–F'	-	-	-0.2836

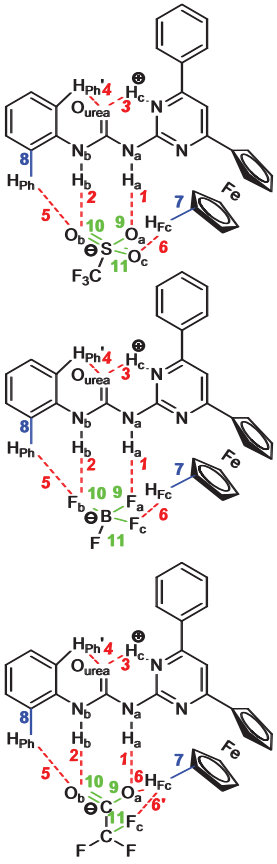

[a] The “free” C—H bonds listed are typical bonds in the phenyl and c-pentadienyl groups.
[b] These bonds involve the unmarked F atoms of $[BF_4]^-$ and $[CF_3CO_2]^-$.

negative values which seem not to correlate with any other parameter and can be considered as noise that originates from the approximate nature of the partitioning. For conventional covalent bonds between second-row elements, the exchange components are in the order of −0.2 to –0.4 E_H, depending on the environment. The C—H exchange contribution is typically between −0.25 and − 0.28 E_H; the N—H contributions are similar in magnitude (note that in our complexes all of them are involved in hydrogen bonds; in some other simple compounds we obtained also similar values for O—H and F—H bonds). There are three well-defined N–H–X (X = O,F) hydrogen bonds in each of the complexes of anions with conformer **a** of the host molecule: two bridges between the anion and the urea nitrogen atoms (marked 1 and 2 in Table 5) and one between the carbonyl O atom and the close-lying N atom of the pyrimidine ring (bond 3 in the Table). The diatomic exchange contribution characterizing the X—H(—Y) bonds is as large as one tenth of those of the conventional covalent X–H bonds. This shows that the exchange energy contribution well represents the (although limited) electron sharing between X and H. The relative magnitude of these bond contributions strongly correlates with the length of the bond (for example, in the $[BF_4]^-$ complex the lengths of bonds 1 and 2 are 1.588 Å and 1.738 Å vs. the respective exchange contributions of −0.0383 E_H and − 0.0266 E_H). The X—H(—C) bonds (4, 5 and 6 in Table 5) seen to exist according to the bond order, QTAIM and NCI analysis have exchange energy components about one order of magnitude smaller in absolute value than the well-defined X—H(—Y) bonds, but well beyond being in the "noise" category. They are larger in absolute value for the C—H bonds of the ferrocene unit (6) than for those involving the phenyl substituent of the urea (4,5). These energy contributions also correlate inversely with the X–H distances.

Notably, the existence of a hydrogen bond between the X and H atoms in a Z-X—H(—Y) (Y=N, C) bridge influences the diatomic exchange energy components of the conventional covalent bonds these atoms are involved: the Z-X (S—O, B—F and C—O) bonds (9–11 in Table 5) and the H—Y bonds (shown only for H—C bonds, 7 and 8 because there are no "free" H—N and H—O bonds in our compounds for reference). If the X atom gets involved in a hydrogen bond (9,10), the magnitude of these contributions decreases (the available reference values are listed in the bottom line of Table 5), and the reduction is larger when the X—H bond is stronger (i.e., its Mayer bond order is larger and its exchange energy contribution is more negative), as if some exchange energy were transferred from the covalent bond to the hydrogen bond. The tendency is the same when the Z-X bond is involved in a Z-X—H(—C) bond (11 in Table 5.) For C—H bonds, the exchange contributions of "free" C—H bonds (listed only for some typical bonds in the phenyl and c-pentadienyl groups) are about −0.273 E_H, but if the bond is involved in hydrogen bond, the contribution is about −0.267 E_H for phenyl C—H bonds that are relatively weaker and less negative than about −0.26 E_H for ferrocene C—H bonds which are stronger. The reduction of the magnitude of exchange energy components is generally much larger than the "strength" of the related hydrogen bond. The difference is probably absorbed in the atomic contributions which also systematically vary depending on the presence or absence of a hydrogen bond.

In summary, the exchange contributions obtained in the chemical energy component analysis also confirm the existence of hydrogen bonds between the anion and the ferrocene as well as phenyl units in the host molecule, and their magnitude reflects the strength of these bonds.

3.5. ^1H NMR experiments and calculations

The electronic structure calculations indicate that there exists an interaction between the ferrocene unit and the electronegative atoms of the anion. This offers a challenge to the experimental studies. Notably, our previous room-temperature ^1H NMR titration studies proved the binding of anions to the ureido group of **S**, but no indication of anion-ferrocene interaction could be observed in those ^1H NMR spectra. As the hydrogen bonds between the anion and the ferrocene unit are considered to contribute to the high affinity of our receptor towards anions of strong acids, it would be desirable to detect the existence of such interactions experimentally. To this end, new ^1H NMR titration experiments were carried out, this time at lower temperatures than in our earlier work. We expected that the signatures of anion-ferrocene interactions should appear by cooling the solution because the conformational changes taking place in the sample solution slow down. The ^1H NMR spectrum of **S**, recorded at 223 K shows two sets of signals, corresponding to the two stable conformers **Sa** and **Sb** with the ferrocene unit positioned close to, and far from the binding site, respectively (see Scheme 3 and Fig. 6). In the range of chemical shifts characteristic to the protons of the ferrocene moiety, one expects to find three groups of peaks corresponding to the five protons of the unsubstituted cyclopentadienyl ring, and to the two α- and to the two β protons of the cyclopentadienyl ring connected to the pyrimidine ring, respectively. The structural differences of the isomers can be expected to cause a minor deviation in the chemical shifts of the protons of the substituted cyclopentadienyl ring and even less difference for those of the unsubstituted Cp ring. The singlet peak found at 4.12 ppm with an area of 5H offers itself to correspond to the five protons of the unsubstituted cyclopentadienyl ring. Based on earlier experience [72] the peaks at 4.59 and 4.63 ppm can be associated with the β protons of the substituted cyclopentadienyl rings that are in somewhat different environment in conformers **Sa** and **Sb**, while the α protons of both conformers appear at 5.00 ppm. Addition of strong acids like triflic acid or HBF_4 to the sample induces characteristic changes in the low-temperature NMR spectrum. Fig. 6 shows the titration of our host molecule by triflic acid, and Fig. S1 demonstrates the analogous changes during titration by HBF_4*Et_2O.

With increasing concentration of either acid, the intensities of the ferrocene signals gradually decrease and simultaneously seven new peaks appear in the range of 3.8 to 5.6 ppm. There are two possible reasons for the appearance of the new peaks. On the one hand, two different isomers of the complexes can be formed, **[SaH] [OTf]** and **[SbH] [OTf]**, that results in two sets of ferrocene signals (see the top panel of Fig. 6). On the other hand, the electronic structure calculations suggest that the electron-deficient ferrocene moiety can be bound by hydrogen bonds to the guest anion (in the case of **[SaH]** $^+$) or to the O atom of the urea group (in the case of **[SbH]** $^+$), which can also cause differences in the chemical shifts of ferrocene protons.

Since no experimental data was available in the literature for similar complexes that could help assigning the measured spectra, we calculated ^1H NMR spectra for the lowest-energy DFT structures (described in detail in section entitled "*Structure of the complexes – Evaluation of secondary interactions*") of **Sa**, **Sb** and the complexes **[SaH] [OTf]**, **[SaH] [BF_4]**, **[SbH] [OTf]** and **[SbH] [BF_4]** (Table 6 and Table S10). The calculated ^1H NMR spectra of **Sa** and **Sb** confirm the qualitative assignment shown above. Five different chemical shift values were found that correspond to the unsubstituted cyclopentadienyl ring of ferrocene. In the experimental spectra the signals of these five protons are not resolved; they merge into the huge singlet peak at 4.12 ppm (with the integral value of 5H). This suggests that the rotation of the cyclopentadienyl ligand is so fast even at the low temperature (223 K) of the measurement that the NMR method is not able to distinguish the different protons. This is in agreement with the low-energy barrier of the Cp rotation in the free ferrocene molecule determined experimentally [104]. The calculations also support the assignment of the peaks at higher and lower chemical shifts to the α- and β-protons, respectively. The changes in the spectra induced by titration by triflic acid can be explained using the calculations on the acid–receptor complexes. Firstly, the difference between the chemical shifts of the two singlets of the protons of the unsubstituted cyclopentadienyl ring in the complexes **[SaH] [OTf]** and **[SbH] [OTf]** is increased compared to **Sa** and **Sb**, leading to splitting of the original peak as it is visible on Fig. 6. Secondly, the heights of the two peaks in the experimental spectrum also differ:

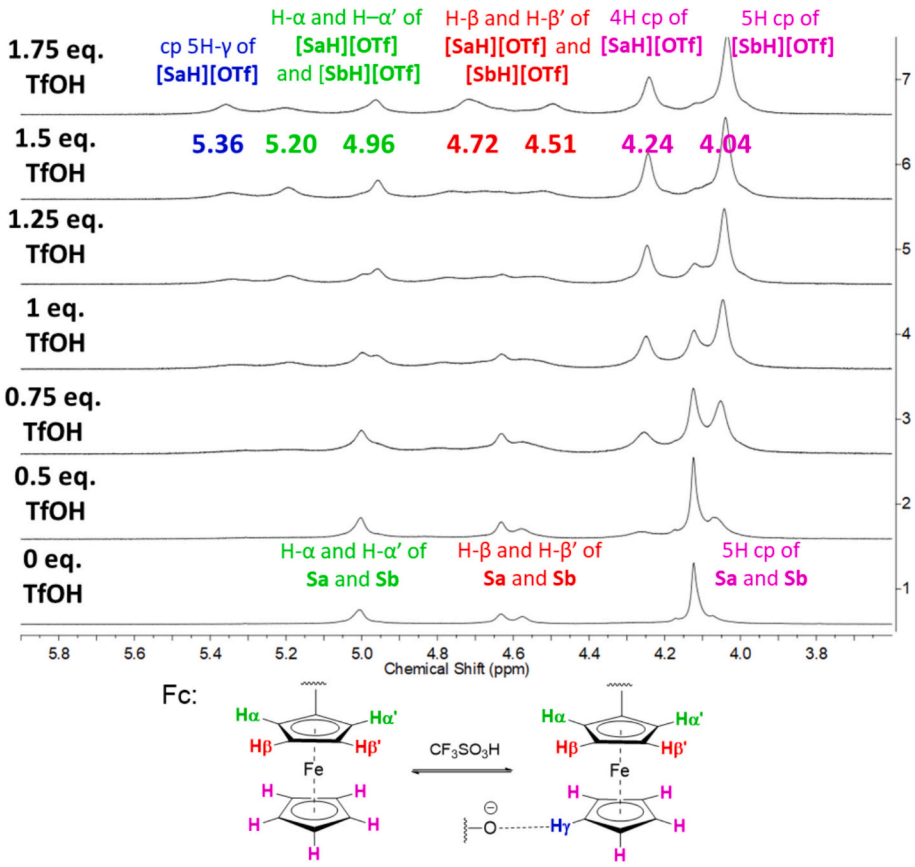

Fig. 6. Changes in the low temperature (223*K*) ^{1}H NMR spectrum of **S** (8.5 mM) during the addition of TfOH (0 ➔ 14.8 mM) in the chemical shift range corresponding to the ferrocene protons. The different proton sites are distinguished by color-coding shown in the bottom structural formulas.

Table 6
Calculated ^{1}H chemical shifts of ferrocene protons in compounds **Sa** and **Sb** as well as in complexes **[SaH] [OTf]** and **[SbH] [OTf]**.

	Sa	Sb	[SaH][OTf]	[SbH][OTf]
	3.27	3.37	3.19	3.42
	3.75	3.85	3.58	3.74
cp 5H	3.84	3.90	3.90	4.09
	3.94	4.01	3.95	4.10
	4.18	4.32		4.64
cp 5H-γ	-	-	5.81	-
cp 2H α	4.71	4.71	4.68	4.61
	5.18	5.26	5.78	4.51
cp 2H β	4.25	4.32	4.43	4.44
	4.27	4.32	4.59	4.51

there is a 4H singlet at 4.24 ppm and a 5H singlet at 4.04 ppm. The latter corresponds to five protons that remain indistinguishable upon complexation. These must be in a freely rotating unsubstituted cyclopentadienyl ring, that of **[SbH] [OTf]**. The 4H peak can be associated

with a cyclopentadienyl ring whose four protons are in essentially identical environment, and one is distinguished from them, which can be associated with the unsubstituted ring in **[SaH] [OTf]** . The location of the "missing" proton can be found by the analysis of the δ_H values obtained in DFT calculations (Table 6, right two columns), according to which the protons in the unsubstituted cyclopentadienyl ligand are almost insensitive to the addition of the acid, except one (denoted cp 5H-γ, Table 6), whose signal is shifted downfield to the highest δ_H value, 5.81 ppm among the ferrocene protons. This calculated peak can be associated with the 5.36 ppm experimental ^{1}H peak that appeared during the titration. According to the calculations, the distinguished proton is in the unsubstituted cyclopentadienyl ring of ferrocene in the **[SaH] [OTf]** conformer, and it participates in the C-H-O bond between the ring and the triflate anion. The 4H peak at 4.24 ppm should belong to the remaining four cp protons in this conformer and the 5H peak at 4.04 ppm to the cp protons in the **[SbH] [OTf]** conformer. The 5H area of the latter peak suggests that the unsubstituted ring in conformer **b** rotates essentially freely, which is in agreement with its calculated structure. (Note that the hydrogen bond between cp and the carbonyl oxygen mentioned above is not strong enough to prevent this rotation even at the low temperature of the NMR experiments.)

The pronounced shift of the signal of the γ proton indicates the existence of a hydrogen bond between ferrocene and triflate anion, thus providing experimental evidence of the hydrogen bond formation shown in section entitled "*Structure of the complexes – Evaluation of secondary interactions*".

Following the tendencies observed in the calculated ^{1}H NMR spectra, it can be determined that the peaks in the range of 4.8 to 4.4 ppm must belong to the β and β' protons of the substituted cyclopentadienyl ring of ferrocene in both conformers **a** and **b** of the complexes. At the chemical shift of 4.96 ppm another singlet peak can be observed, which can be assigned to the α and α' protons of **[SbH] [OTf]** and the α' proton of **[SaH] [OTf]** based on the proximity of the calculated δ_H values to each other. Somewhat surprisingly, the calculations suggest that the remaining peak at 5.20 ppm in the experimental spectrum belongs to the α proton of conformer **a**. this large shift can be caused by the formation of another weak hydrogen bond between the ferrocene α proton and the guest anion. The titration experiments carried out with HBF_4*Et_2O provided essentially the same results (Fig. S1, Scheme S1 and. Table S10)

4. Conclusion

In our investigation into the factors contributing to the relatively strong binding of weakly coordinating anions to the ferrocene-decorated receptor S, we observed the presence of various secondary hydrogen bonds that play a crucial role in stabilizing these complexes. One particularly remarkable interaction is the C_{sp2}-H—O(F) bond involving the ferrocene moiety, which was originally incorporated into the molecule solely to serve as an electrochemical marker for the detection of anions. Urea moieties are typically excellent binding sites for carboxylate anions due to their matching geometries. We observed that even when the binding to the urea binding site is less favorable due to improper geometry or weak basicity for anions like $[OTf]^-$ or $[BF_4]^-$, the possibility of the formation of ferrocene mediated hydrogen bonds enhances complexation. The detailed analysis of geometries calculated with electronic structure methods suggested the presence of such interactions. Semiquantitative quantum chemical tools confirmed the existence of hydrogen bonds involving the ferrocene moiety. Remarkably, an experimental proof for the theoretical predictions was provided by low temperature ^{1}H NMR titration experiments. The results suggest that ferrocene is not a completely innocent constituent of electrochemically detectable acid receptors, and the proper application of ferrocene side-chains in newly designed molecular receptors can mean a great advantage in the sensing of weakly coordinating anions

CRediT authorship contribution statement

Soma Keszei: Writing – review & editing, Writing – original draft, Visualization, Methodology, Investigation, Conceptualization. **Rita Skoda-Földes:** Writing – review & editing, Resources, Funding acquisition. **György Lendvay:** Writing – review & editing, Supervision, Software, Investigation, Conceptualization.

Declaration of competing interest

The authors declare that they have no known competing financial interests or personal relationships that could have appeared to influence the work reported in this paper.

Acknowledgements

We are grateful to Szabolcs Balogh for his help with the NMR measurements. This study has been supported by the NRDI (National Research Excellence Programme, No.: ADVANCED 149644).

Appendix A. Supplementary data

Supplementary data to this article can be found online at https://doi.org/10.1016/j.molliq.2026.129292.

Data availability

The data that supports the findings of this study are available in the Supporting Information of this article.

References

[1] C.H. Park, Simmons, H.E. Macrobicyclic Amines, III. Encapsulation of Halide Ions by in,in-1,(k + 2)-Diazabicyclo[k.l.m.]Alkane Ammonium Ions, J. Am. Chem. Soc. 90 (9) (1968) 2431–2432, https://doi.org/10.1021/ja01011a047.
[2] P.D. Beer, P.A. Gale, Anion recognition and sensing: the state of the art and future perspectives, Angew. Chem. Int. Ed. 40 (3) (2001) 486–516, https://doi.org/10.1002/1521-3773(20010202)40:3%253C486::AID-ANIE486%253E3.0.CO;2-P.
[3] J.W. Steed, Coordination and organometallic compounds as anion receptors and sensors, Chem. Soc. Rev. 38 (2) (2009) 506–519, https://doi.org/10.1039/B810364J.
[4] P.A. Gale, N. Busschaert, C.J.E. Haynes, L.E. Karagiannidis, I.L. Kirby, Anion receptor chemistry: highlights from 2011 and 2012, Chem. Soc. Rev. 43 (1) (2014) 205–241, https://doi.org/10.1039/C3CS60316D.
[5] N.H. Evans, P.D. Beer, Advances in anion supramolecular chemistry: from recognition to chemical applications, Angew. Chem. Int. Ed. 53 (44) (2014) 11716–11754, https://doi.org/10.1002/anie.201309937.
[6] K.-C. Chang, S.-S. Sun, M.O. Odago, A.J. Lees, Anion recognition and sensing by transition-metal complexes with polarized N H recognition motifs, Coord. Chem. Rev. 284 (2015) 111–123, https://doi.org/10.1016/j.ccr.2014.09.009.
[7] P.A. Gale, C. Caltagirone, Anion sensing by small molecules and molecular ensembles, Chem. Soc. Rev. 44 (13) (2015) 4212–4227, https://doi.org/10.1039/C4CS00179F.
[8] P.A. Gale, E.N.W. Howe, X. Wu, Anion receptor chemistry, Chem 1 (3) (2016) 351–422, https://doi.org/10.1016/j.chempr.2016.08.004.
[9] L. Chen, S.N. Berry, X. Wu, E.N.W. Howe, P.A. Gale, Advances in anion receptor chemistry, Chem 6 (1) (2020) 61–141, https://doi.org/10.1016/j.chempr.2019.12.002.
[10] L.K. Macreadie, A.M. Gilchrist, D.A. McNaughton, W.G. Ryder, M. Fares, P. A. Gale, Progress in anion receptor chemistry, Chem 8 (1) (2022) 46–118, https://doi.org/10.1016/j.chempr.2021.10.029.
[11] D.A. McNaughton, W.G. Ryder, A.M. Gilchrist, P. Wang, M. Fares, X. Wu, P. A. Gale, New insights and discoveries in anion receptor chemistry, Chem 9 (11) (2023) 3045–3112, https://doi.org/10.1016/j.chempr.2023.07.006.
[12] P. Molina, F. Zapata, A. Caballero, Anion recognition strategies based on combined noncovalent interactions, Chem. Rev. 117 (15) (2017) 9907–9972, https://doi.org/10.1021/acs.chemrev.6b00814.
[13] N. Kaur, G. Kaur, U.A. Fegade, A. Singh, S.K. Sahoo, A.S. Kuwar, N. Singh, Anion sensing with Chemosensors having multiple NH recognition units, TrAC Trends Anal. Chem. 95 (2017) 86–109, https://doi.org/10.1016/j.trac.2017.08.003.
[14] S.J. Coles, G. Denuault, P.A. Gale, P.N. Horton, M.B. Hursthouse, M.E. Light, C. N. Warriner, Mono- and bis-ferrocene 2,5-Diamidopyrrole clefts: solid-state assembly, Anion Binding and Electrochemical Properties. Polyhedron 22 (5) (2003) 699–709, https://doi.org/10.1016/S0277-5387(02)01401-8.

[15] S. Camiolo, P.A. Gale, M.B. Hursthouse, M.E. Light, Nitrophenyl derivatives of pyrrole 2,5-diamides: structural behaviour, anion binding and colour change signalled deprotonationElectronic supplementary information (ESI) available: 1H NMR, 13C NMR and mass spectra for compounds 2 and 3, NMR anion titration profiles in DMSO-D6–0.5% water. See Http://Www.Rsc.Org/Suppdata/Ob/B2/B210848h/, Org. Biomol. Chem. 1 (4) (2003) 741–744, https://doi.org/10.1039/b210848h.

[16] C.-L. Chen, Y.-H. Chen, C.-Y. Chen, S.-S. Sun, Dipyrrole carboxamide derived selective Ratiometric probes for cyanide ion, Org. Lett. 8 (22) (2006) 5053–5056, https://doi.org/10.1021/ol061969g.

[17] V. Amendola, M. Boiocchi, L. Fabbrizzi, A. Palchetti, What anions do inside a receptor's cavity: a trifurcate anion receptor providing both electrostatic and hydrogen-bonding interactions, Chemistry A European J 11 (19) (2005) 5648–5660, https://doi.org/10.1002/chem.200500351.

[18] N. Luo, J. Li, T. Sun, S. Wan, P. Li, N. Wu, Y. Yan, X. Bao, Carbazole Sulfonamide-based macrocyclic receptors capable of selective complexation of fluoride ion, RSC Adv. 11 (17) (2021) 10203–10211, https://doi.org/10.1039/D1RA01285A.

[19] G. Picci, R. Montis, V. Lippolis, C. Caltagirone, Squaramide-based receptors in anion supramolecular chemistry: insights into anion binding, sensing, Transport and Extraction. *Chem. Soc. Rev.* 53 (8) (2024) 3952–3975, https://doi.org/10.1039/D3CS01165H.

[20] C. Caltagirone, G.W. Bates, P.A. Gale, M.E. Light, Anion binding vs.Sulfonamide deprotonation in functionalised Ureas, Chem. Commun. 1 (2008) 61–63, https://doi.org/10.1039/B713431B.

[21] J.-L. Fillaut, J. Andriès, J. Perruchon, J.-P. Desvergne, L. Toupet, L. Fadel, B. Zouchoune, J.-Y. Saillard, Alkynyl ruthenium colorimetric sensors: optimizing the selectivity toward fluoride anion, Inorg. Chem. 46 (15) (2007) 5922–5932, https://doi.org/10.1021/ic062389i.

[22] T. Gunnlaugsson, P.E. Kruger, T.C. Lee, R. Parkesh, F.M. Pfeffer, G.M. Hussey, Dual responsive Chemosensors for anions: the combination of fluorescent PET (photoinduced Electron transfer) and colorimetric Chemosensors in a single molecule, Tetrahedron Lett. 44 (35) (2003) 6575–6578, https://doi.org/10.1016/S0040-4039(03)01699-X.

[23] R.B.P. Elmes, T. Gunnlaugsson, Luminescence anion sensing via modulation of MLCT emission from a Naphthalimide–Ru(II)–polypyridyl complex, Tetrahedron Lett. 51 (31) (2010) 4082–4087, https://doi.org/10.1016/j.tetlet.2010.05.127.

[24] S. Guha, S. Saha, Fluoride ion sensing by an anion−π interaction, J. Am. Chem. Soc. 132 (50) (2010) 17674–17677, https://doi.org/10.1021/ja107382x.

[25] H.E. Katz, Hydride sponge: complexation of 1,8-Naphthalenediylbis(Dimethylborane) with hydride, fluoride, and hydroxide, J. Org. Chem. 50 (25) (1985) 5027–5032, https://doi.org/10.1021/jo00225a005.

[26] Williams, V. C.; Piers, W. E.; Clegg, W.; Elsegood, M. R. J.; Collins, S.; Marder, T. B. New Bifunctional Perfluoroaryl Boranes. Synthesis and Reactivity of the *Ortho*-Phenylene-Bridged Diboranes 1,2-[B(C_6F_5)$_2$]$_2$$C_6X_4$ (X = H, F)'. *J. Am.* Chem. Soc. 1999, 121 (13), 3244–3245. doi:https://doi.org/10.1021/ja990082v.

[27] S. Yamaguchi, S. Akiyama, K. Tamao, Colorimetric fluoride ion sensing by boron-containing π-Electron systems, J. Am. Chem. Soc. 123 (46) (2001) 11372–11375, https://doi.org/10.1021/ja015957w.

[28] S. Yamaguchi, T. Shirasaka, S. Akiyama, K. Tamao, Dibenzoborole-containing π-Electron systems: remarkable fluorescence change based on the "on/off" control of the $p_\pi-\pi^*$ conjugation, J. Am. Chem. Soc. 124 (30) (2002) 8816–8817, https://doi.org/10.1021/ja026689k.

[29] Y. Kubo, M. Yamamoto, M. Ikeda, M. Takeuchi, S. Shinkai, S. Yamaguchi, K. Tamao, A colorimetric and Ratiometric fluorescent Chemosensor with three emission changes: fluoride ion sensing by a Triarylborane– porphyrin conjugate, Angew. Chem. Int. Ed. 42 (18) (2003) 2036–2040, https://doi.org/10.1002/anie.200250788.

[30] J.D.E. Lane, S.N. Berry, W. Lewis, J. Ho, K.A. Jolliffe, Diaminomethylenemalononitriles and Diaminomethyleneindanediones as dual hydrogen bond donors for anion recognition, J. Org. Chem. 86 (7) (2021) 4957–4964, https://doi.org/10.1021/acs.joc.0c02801.

[31] M.T. Reetz, C.M. Niemeyer, K. Harms, Crown ethers with a Lewis acidic Center: a new class of heterotopic host molecules, Angew. Chem. Int. Ed. Engl. 30 (11) (1991) 1472–1474, https://doi.org/10.1002/anie.199114721.

[32] C.R. Cooper, Selective fluorescence detection of fluoride using boronic acids, Chem. Commun. 13 (1998) 1365–1366, https://doi.org/10.1039/a801693c.

[33] P. Dydio, D. Lichosyt, J. Jurczak, Amide- and urea-functionalized pyrroles and Benzopyrroles as synthetic, neutral anion receptors, Chem. Soc. Rev. 40 (5) (2011) 2971, https://doi.org/10.1039/c1cs15006e.

[34] V. Blažek Bregović, N. Basarić, K. Mlinarić-Majerski, Anion binding with urea and thiourea derivatives, Coord. Chem. Rev. 295 (2015) 80–124, https://doi.org/10.1016/j.ccr.2015.03.011.

[35] H. Miyaji, S.R. Collinson, I. Prokeš, J.H.R. Tucker, A Ditopic ferrocene receptor for anions and cations that functions as a chromogenic molecular switch, Chem. Commun. 1 (2003) 64–65, https://doi.org/10.1039/B210227G.

[36] Á. Lorenzo, E. Aller, P. Molina, Iminophosphorane-based synthesis of multinuclear Ferrocenyl urea, thiourea and guanidine derivatives and exploration of their anion sensing properties, Tetrahedron 65 (7) (2009) 1397–1401, https://doi.org/10.1016/j.tet.2008.12.030.

[37] Y. Willener, K.M. Joly, C.J. Moody, J.H.R. Tucker, An exploration of Ferrocenyl Ureas as enantioselective electrochemical sensors for chiral carboxylate anions, J. Org. Chem. 73 (4) (2008) 1225–1233, https://doi.org/10.1021/jo701809b.

[38] C.M.G. Dos Santos, T. McCabe, G.W. Watson, P.E. Kruger, T. Gunnlaugsson, The recognition and sensing of anions through "positive allosteric effects" using simple urea−amide receptors, J. Org. Chem. 73 (23) (2008) 9235–9244, https://doi.org/10.1021/jo8014424.

[39] S. Rashdan, M.E. Light, J.D. Kilburn, Pyridyl thioureas as switchable anion receptors, Chem. Commun. No. 44 (2006) 4578, https://doi.org/10.1039/b611138f.

[40] L.M. Jordan, P.D. Boyle, A.L. Sargent, W.E. Allen, Binding of carboxylic acids by fluorescent pyridyl Ureas, J. Org. Chem. 75 (24) (2010) 8450–8456, https://doi.org/10.1021/jo101730w.

[41] S.J. Keszei, M. Váradi, R. Skoda-Földes, Urea-functionalized heterocycles: structure, hydrogen bonding and applications, Molecules 28 (23) (2023) 7757, https://doi.org/10.3390/molecules28237757.

[42] Gunnlaugsson, T.; Glynn, M.; Tocci (Née Hussey), G. M.; Kruger, P. E.; Pfeffer, F. M. Anion recognition and sensing in organic and aqueous media using luminescent and colorimetric sensors. Coord. Chem. Rev. 2006, 250 (23–24), 3094–3117. doi:https://doi.org/10.1016/j.ccr.2006.08.017.

[43] L.E. Santos-Figueroa, M.E. Moragues, E. Climent, A. Agostini, R. Martínez-Máñez, F. Sancenón, Chromogenic and fluorogenic Chemosensors and reagents for anions. A comprehensive review of the years 2010–2011, Chem. Soc. Rev. 42 (8) (2013) 3489, https://doi.org/10.1039/c3cs35429f.

[44] P.A. Gale, C. Caltagirone, Fluorescent and colorimetric sensors for anionic species, Coord. Chem. Rev. 354 (2018) 2–27, https://doi.org/10.1016/j.ccr.2017.05.003.

[45] D.A. McNaughton, M. Fares, G. Picci, P.A. Gale, C. Caltagirone, Advances in fluorescent and colorimetric sensors for anionic species, Coord. Chem. Rev. 427 (2021) 213573, https://doi.org/10.1016/j.ccr.2020.213573.

[46] G. Picci, R. Montis, A.M. Gilchrist, P.A. Gale, C. Caltagirone, Fluorescent and colorimetric sensors for anions: highlights from 2020 to 2022, Coord. Chem. Rev. 501 (2024) 215561, https://doi.org/10.1016/j.ccr.2023.215561.

[47] Beer, P. D.; Bayly, S. R. Anion Sensing by Metal-Based Receptors. In *Anion Sensing*; Stibor, I., Ed.; Topics in Current Chemistry; Springer Berlin Heidelberg: Berlin, Heidelberg, 2005; Vol. 255, pp 125–162. doi:https://doi.org/10.1007/b101165.

[48] P. Beer, Electrochemical and optical sensing of anions by transition metal based receptors, Coord. Chem. Rev. 205 (1) (2000) 131–155, https://doi.org/10.1016/S0010-8545(00)00237-X.

[49] T. Romero, R.A. Orenes, A. Tárraga, P. Molina, Preparation, structural characterization, electrochemistry, and sensing properties toward anions and cations of ferrocene-triazole derivatives, Organometallics 32 (20) (2013) 5740–5753, https://doi.org/10.1021/om4002457.

[50] Zapata, F.; Caballero, A.; Molina, P. Ferrocene–Triazole Combination as a Benchmark for the Electrochemical Detection of Noncovalent Halogen-Bonding Interactions. Eur. J. Inorg. Chem. 2017, 2017 (2), 237–241. doi:https://doi.org/10.1002/ejic.201600838.

[51] P.D. Beer, P.A. Gale, G.Z. Chen, Mechanisms of electrochemical recognition of cations, anions and neutral guest species by redox-active receptor molecules, Coord. Chem. Rev. 185–186 (1999) 3–36, https://doi.org/10.1016/S0010-8545(98)00246-X.

[52] P.D. Beer, P.A. Gale, Z. Chen, Electrochemical recognition of charged and neutral guest species by redox-active receptor molecules, in: Advances in Physical Organic Chemistry vol. 31, Elsevier, 1999, pp. 1–90, https://doi.org/10.1016/S0065-3160(08)60192-6.

[53] Q.-Y. Cao, T. Pradhan, S. Kim, J.S. Kim, Ferrocene-appended aryl triazole for electrochemical recognition of phosphate ions, Org. Lett. 13 (16) (2011) 4386–4389, https://doi.org/10.1021/ol201722d.

[54] F. Otón, A. Tárraga, A. Espinosa, M.D. Velasco, P. Molina, Ferrocene-based Ureas as Multisignaling receptors for anions, J. Org. Chem. 71 (12) (2006) 4590–4598, https://doi.org/10.1021/jo0604540.

[55] D.A. Jose, D.K. Kumar, B. Ganguly, A. Das, Urea and thiourea based efficient colorimetric sensors for oxyanions, Tetrahedron Lett. 46 (32) (2005) 5343–5346, https://doi.org/10.1016/j.tetlet.2005.06.011.

[56] S. Sasaki, M. Mizuno, K. Naemura, Y. Tobe, Synthesis and anion-selective complexation of cyclophane-based cyclic thioureas, J. Org. Chem. 65 (2) (2000) 275–283, https://doi.org/10.1021/jo991237k.

[57] J.-S. Wu, H.J. Kim, M.H. Lee, J.H. Yoon, J.H. Lee, J.S. Kim, Anion-induced ring-opening of fluorescein Spirolactam: fluorescent OFF–ON, Tetrahedron Lett. 48 (18) (2007) 3159–3162, https://doi.org/10.1016/j.tetlet.2007.03.060.

[58] W.-X. Liu, Y.-B. Jiang, N-Amidothiourea based PET Chemosensors for anions, Org. Biomol. Chem. 5 (11) (2007) 1771, https://doi.org/10.1039/b703122j.

[59] J.H. Oh, B.P. Hay, V.M. Lynch, H. Li, J.L. Sessler, S.K. Kim, Calix[4]pyrrole-based molecular capsule: dihydrogen phosphate-promoted 1:2 fluoride anion complexation, J. Am. Chem. Soc. 144 (37) (2022) 16996–17009, https://doi.org/10.1021/jacs.2c06284.

[60] P. Bhandari, P.S. Mukherjee, Post-synthesis conversion of an unstable imine cage to a stable cage with amide moieties towards selective receptor for fluoride, Chemistry A European J 28 (57) (2022) e202201901, https://doi.org/10.1002/chem.202201901.

[61] Mondal, D.; Ahmad, M.; Panwaria, P.; Upadhyay, A.; Talukdar, P. Anion Recognition through Multivalent C–H Hydrogen Bonds: Anion-Induced Foldamer Formation and Transport across Phospholipid Membranes. J. Org. Chem. 2022, 87 (1), 10–17. doi:https://doi.org/10.1021/acs.joc.1c01408.

[62] F. Pan, N.K. Beyeh, S. Bertella, K. Rissanen, Anion-exchange properties of trifluoroacetate and triflate salts of *N*-alkylammonium Resorcinarenes, Chemistry An Asian Journal 11 (5) (2016) 782–788, https://doi.org/10.1002/asia.201501335.

[63] C. Guérin, Z. Zhang, L. Jean-Gérard, S. Steinmann, C. Michel, B. Andrioletti, Strong affinity of triazolium-appended Dipyrromethenes (TADs) for BF4−, Molecules 25 (19) (2020) 4555, https://doi.org/10.3390/molecules25194555.

[64] X. Gong, Q.-L. Zhang, S. Zhang, Y. Xia, Q. Bai, S. Chen, X.-L. Ni, A cationic fluorescent probe for BF4− and PF6− anions by aggregation self-assembly: an

efficient approach to recognition of anions in aqueous solution, Dyes Pigments 163 (2019) 502–508, https://doi.org/10.1016/j.dyepig.2018.12.038.
[65] I. Krossing, I. Raabe, Noncoordinating anions—fact or fiction? A survey of likely candidates, Angew. Chem. Int. Ed. 43 (16) (2004) 2066–2090, https://doi.org/10.1002/anie.200300620.
[66] J. Cai, J.L. Sessler, Neutral CH and cationic CH donor groups as anion receptors, Chem. Soc. Rev. 43 (17) (2014) 6198–6213, https://doi.org/10.1039/C4CS00115J.
[67] Eytel, L. M.; Gilbert, A. K.; Görner, P.; Zakharov, L. N.; Johnson, D. W.; Haley, M. M. Do CH–Anion and Anion–π Interactions Alter the Mechanism of 2:1 Host–Guest Complexation in Arylethynyl Monourea Anion Receptors? Chemistry A European J 2017, 23 (17), 4051–4054. doi:https://doi.org/10.1002/chem.201605452.
[68] F. Zapata, L. Gonzalez, A. Caballero, I. Alkorta, J. Elguero, P. Molina, Dual role of the 1,2,3-triazolium ring as a hydrogen-bond donor and anion–π receptor in anion-recognition processes, Chemistry A European J 21 (27) (2015) 9797–9808, https://doi.org/10.1002/chem.201500231.
[69] F. Zapata, A. Caballero, A. Espinosa, A. Tárraga, P. Molina, Cation coordination induced modulation of the anion sensing properties of a ferrocene−Imidazophenanthroline dyad: multichannel recognition from phosphate-related to chloride anions, J. Org. Chem. 73 (11) (2008) 4034–4044, https://doi.org/10.1021/jo800296c.
[70] P.A. Gale, M.B. Hursthouse, M.E. Light, J.L. Sessler, C.N. Warriner, R. S. Zimmerman, Ferrocene-substituted calix[4]pyrrole: a new electrochemical sensor for anions involving CH···anion hydrogen bonds, Tetrahedron Lett. 42 (38) (2001) 6759–6762, https://doi.org/10.1016/S0040-4039(01)01337-5.
[71] S.R. Beeren, J.K.M. Sanders, Discovery of linear receptors for multiple dihydrogen phosphate ions using dynamic combinatorial chemistry, J. Am. Chem. Soc. 133 (11) (2011) 3804–3807, https://doi.org/10.1021/ja200130h.
[72] S.J. Keszei, S. Balogh, C. Fehér, L. Nagy, N. Tumanov, J. Wouters, G. Lendvay, R. Skoda-Földes, Molecular recognition of strong acids by using a 2-Ureido-4-Ferrocenyl pyrimidine receptor, Eur J Inorg Chem 2019 (38) (2019) 4095–4104, https://doi.org/10.1002/ejic.201900803.
[73] Gaussian 09, Revision A.02; Gaussian, Inc.: Wallingford, CT, 2009.
[74] Yanai, T.; Tew, D. P.; Handy, N. C. A New Hybrid Exchange–Correlation Functional Using the Coulomb-Attenuating Method (CAM-B3LYP). Chemical Physics Letters 2004, 393 (1–3), 51–57. doi:https://doi.org/10.1016/j.cplett.2004.06.011.
[75] R.L. Martin, Natural transition orbitals, J. Chem. Phys. 118 (11) (2003) 4775–4777, https://doi.org/10.1063/1.1558471.
[76] C. Fehér, M. Papp, Á. Gömöry, L. Nagy, J. Wouters, G. Lendvay, R. Skoda-Földes, Synthesis of 2-Ureido-4-Ferrocenyl pyrimidine guests. Investigation of complementary molecular recognition of 2,6-Diaminopyridine, Organometallics 35 (24) (2016) 4023–4032, https://doi.org/10.1021/acs.organomet.6b00586.
[77] R. Ditchfield, Self-consistent perturbation theory of diamagnetism: I. A gauge-invariant LCAO method for N.M.R. Chemical shifts, Molecular Physics 27 (4) (1974) 789–807, https://doi.org/10.1080/00268977400100711.
[78] H.F. Hameka, On the nuclear magnetic shielding in the hydrogen molecule, Molecular Physics 1 (3) (1958) 203–215, https://doi.org/10.1080/00268975800100261.
[79] K. Wolinski, J.F. Hinton, P. Pulay, Efficient implementation of the gauge-independent atomic orbital method for NMR chemical shift calculations, J. Am. Chem. Soc. 112 (23) (1990) 8251–8260, https://doi.org/10.1021/ja00179a005.
[80] T. Lu, F. Chen, Multiwfn: a multifunctional wavefunction Analyzer, J. Comput. Chem. 33 (5) (2012) 580–592, https://doi.org/10.1002/jcc.22885.
[81] Váradi, M.; Keszei, S. J.; Gömöry, Á.; Kovács, M.; Kégl, T.; Fodor, L.; Skoda-Földes, R. Investigation of Host–Guest Interactions in 2-Ureido-4-Ferrocenylpyrimidine Derivatives. IJMS 2024, 25 (24), 13552. doi:https://doi.org/10.3390/ijms252413552.
[82] P. Hobza, Z. Havlas, Blue-Shifting Hydrogen Bonds, Chem. Rev. 100 (11) (2000) 4253–4264, https://doi.org/10.1021/cr990050q.
[83] E.R. Johnson, S. Keinan, P. Mori-Sánchez, J. Contreras-García, A.J. Cohen, W. Yang, Revealing noncovalent interactions, J. Am. Chem. Soc. 132 (18) (2010) 6498–6506, https://doi.org/10.1021/ja100936w.
[84] R.A. Boto, J. Contreras-García, J. Tierny, J.-P. Piquemal, Interpretation of the reduced density gradient, Mol. Phys. 114 (7–8) (2016) 1406–1414, https://doi.org/10.1080/00268976.2015.1123777.
[85] R.F.W. Bader, A bond path: a universal Indicator of bonded interactions, J. Phys. Chem. A 102 (37) (1998) 7314–7323, https://doi.org/10.1021/jp981794v.
[86] U. Koch, P.L.A. Popelier, Characterization of C-H-O hydrogen bonds on the basis of the charge density, J. Phys. Chem. 99 (24) (1995) 9747–9754, https://doi.org/10.1021/j100024a016.
[87] S.J. Grabowski, Non-covalent interactions – QTAIM and NBO analysis, J. Mol. Model. 19 (11) (2013) 4713–4721, https://doi.org/10.1007/s00894-012-1463-7.
[88] A.V. Afonin, D. Rusinska-Roszak, Quantification of hydrogen bond energy based on equations using spectroscopic, structural, QTAIM-based, and NBO-based descriptors which calibrated by the molecular tailoring approach, J. Mol. Model. 30 (1) (2024) 18, https://doi.org/10.1007/s00894-023-05811-1.
[89] G.S.G. Krishnan, K. Muraleedharan, Unravelling the sensing mechanism of bis-urea macrocycle-based anion receptor: a theoretical study, Supramolecular Materials 4 (2025) 100111, https://doi.org/10.1016/j.supmat.2025.100111.
[90] I.L. Kirby, M. Brightwell, M.B. Pitak, C. Wilson, S.J. Coles, P.A. Gale, Systematic experimental charge density analysis of anion receptor complexes, Phys. Chem. Chem. Phys. 16 (22) (2014) 10943–10958, https://doi.org/10.1039/C3CP54858A.
[91] R.F.W. Bader, H. Essén, The characterization of atomic interactions, J. Chem. Phys. 80 (5) (1984) 1943–1960, https://doi.org/10.1063/1.446956.
[92] I. Rozas, I. Alkorta, J. Elguero, Behavior of ylides containing N, O, and C atoms as hydrogen bond acceptors, J. Am. Chem. Soc. 122 (45) (2000) 11154–11161, https://doi.org/10.1021/ja0017864.
[93] A.D. Becke, K.E. Edgecombe, A simple measure of Electron localization in atomic and molecular systems, J. Chem. Phys. 92 (9) (1990) 5397–5403, https://doi.org/10.1063/1.458517.
[94] H.L. Schmider, A.D. Becke, Chemical content of the kinetic energy density, J. Mol. Struct. (THEOCHEM) 527 (1–3) (2000) 51–61, https://doi.org/10.1016/S0166-1280(00)00477-2.
[95] E. Espinosa, E. Molins, C. Lecomte, Hydrogen bond strengths revealed by topological analyses of experimentally observed Electron densities, Chemical Physics Letters 285 (3–4) (1998) 170–173, https://doi.org/10.1016/S0009-2614(98)00036-0.
[96] J. Andrés, P.W. Ayers, R.A. Boto, R. Carbó-Dorca, H. Chermette, J. Cioslowski, J. Contreras-García, D.L. Cooper, G. Frenking, C. Gatti, F. Heidar-Zadeh, L. Joubert, Á. Martín Pendás, E. Matito, I. Mayer, A.J. Misquitta, Y. Mo, J. Pilmé, P.L.A. Popelier, M. Rahm, E. Ramos-Cordoba, P. Salvador, W.H.E. Schwarz, S. Shahbazian, B. Silvi, M. Solà, K. Szalewicz, V. Tognetti, F. Weinhold, É. Zins, Nine questions on energy decomposition analysis, J. Comput. Chem. 40 (26) (2019) 2248–2283, https://doi.org/10.1002/jcc.26003.
[97] I. Mayer, Improved chemical energy component analysis, Phys. Chem. Chem. Phys. 14 (1) (2012) 337–344, https://doi.org/10.1039/C1CP22476J.
[98] I. Mayer, Energy partitioning schemes, Phys. Chem. Chem. Phys. 8 (40) (2006) 4630, https://doi.org/10.1039/b608822h.
[99] I. Mayer, A chemical energy component analysis, Chem. Phys. Lett. 332 (3–4) (2000) 381–388, https://doi.org/10.1016/S0009-2614(00)01248-3.
[100] I. Mayer, A. Hamza, Interatomic exchange energy components, Int J of Quantum Chemistry 92 (2) (2003) 174–180, https://doi.org/10.1002/qua.10504.
[101] Hamza, A.; Mayer, I. Physical Analysis of the Diatomic "Chemical" Energy Components. *Theoretical Chemistry Accounts: Theory, Computation, and Modeling (Theoretica Chimica Acta)* **2003**, *109* (2), 91–98. doi:https://doi.org/10.1007/s00214-002-0426-y.
[102] I. Bakó, L. Jicsinszky, S. Pothoczki, Systematic study of different types of interactions in α-, β- and γ-cyclodextrin: quantum chemical investigation, Molecules 29 (10) (2024) 2205, https://doi.org/10.3390/molecules29102205.
[103] Http://Occam.Ttk.Hu/Programs/Index.Html. Accessed March 18, 2025.
[104] R.K. Bohn, A. Haaland, On the molecular structure of ferrocene, Fe(C5H5)2, J. Organomet. Chem. 5 (5) (1966) 470–476, https://doi.org/10.1016/S0022-328X(00)82382-7.